High-Performance Dual-View 3-D Display System Based on Integral Imaging

Yan Xing
Qiong-Hua Wang
Ling Luo
Hui Ren
Huan Deng
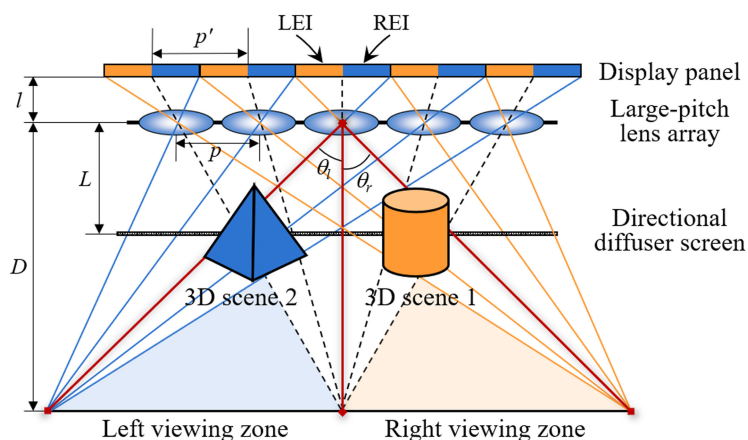
High-Performance Dual-View 3-D Display System Based on Integral Imaging

Yan Xing,[1] **Qiong-Hua Wang** ⓘ**,**[2] **Ling Luo,**[1] **Hui Ren,**[1] **and Huan Deng**[1]

[1]School of Electronics and Information Engineering, Sichuan University, Chengdu 610065, China
[2]School of Instrumentation and Optoelectronic Engineering, Beihang University, Beijing 100191, China

Abstract: In this paper, a dual-view three-dimensional (3-D) display is reported to provide two different high-quality 3-D images in different viewing zones simultaneously. By introducing an improved integral imaging system, which consists of a display panel, a large-pitch lens array, and a directional diffuser screen, two different 3-D images can be reconstructed in different wide viewing zones with high 3-D resolution. In addition, a high accurate pickup method based on projective transformation is presented. A prototype of the proposed dual-view 3-D display is developed and it has good performance.

Index Terms: Dual-view, integral imaging, directional diffuser screen, projective transformation.

1. Introduction

Dual-view display, which provides two distinct images in different viewing regions, recently has triggered much interest in the display field. Apart from changing the structure of the liquid crystal display (LCD) [1]–[4], most conventional dual-view displays use optical components such as lenticular lenses or parallax barriers to show different views to different observers [5], [6], which only present two-dimensional (2D) images. Since the lenticular lenses or the parallax barriers are also the key components of the autostereoscopic three-dimensional (3D) display [7]–[9], the basic principles of the conventional dual-view 2D display and the autostereoscopic 3D display are similar in terms of showing two or more different views. This similarity gives researchers inspiration to design the dual-view 3D display that shows different 3D images by introducing the existing 3D display technologies.

In recent years, several interesting 3D display technologies have been demonstrated, including holographic display [10], light field display [11]–[14], integral imaging (II) display [15]–[19], and volumetric display [20]. Among these technologies, the II display allows the reconstruction of full-parallax and full-color of 3D scene and does not require coherent light or complex system [15], [17]. Because of its good performance for providing continuous viewing 3D images, it is possible to use the II display to create a dual-view 3D display. Some of the pioneering works have already demonstrated

the feasibility of such architecture. Our group has presented a dual-view II 3D display system by dividing the elemental images (EIs) into two parts for the creation of two different viewing zones and subsequently presented an improved dual-view II 3D display system in which two polarizer parallax barriers are added [21], [22]. Both systems show their abilities to reconstruct different 3D images to different viewing zones. However, depending on the conventional adopted II display system, these spatial-multiplexed dual-view II 3D displays suffer from several limitations such as a narrow viewing angle because of the viewing-zone-sharing property between different reconstructed 3D images, or low 3D resolution of the reconstructed 3D images due to the blocking effect of the polarization barriers. A projected-type dual-view II 3D display system has been reported to improve the visibility of the reconstructed 3D images [23]. The system splits the interwoven EIs into different directions by using lenticular lenses and then generates different 3D images in different viewing regions by using high numerical aperture lens array. However, severe black lines appear in the reconstructed 3D images due to the parallaxes separation characteristic of the lenticular lenses. The black lines degrade the quality of each reconstructed 3D image.

Recently, our group has demonstrated a time-multiplexed dual-view II 3D display prototype that improves the viewing angle and the 3D resolution by incorporating two orthogonal polarizer arrays and a polarization switcher [24]. Although the prototype successfully demonstrates the capability of improving the performance of a dual-view II 3D display system, an ultra-high refresh rate is required for showing different 3D images simultaneously. In addition, there are large flipping zones between viewing zones 1 and 2, which degrade the viewing experience. A polarized-glasses-based dual view II 3D display without the limitation of the optimal viewing distance has been presented [25]. However, the observers need to wear the polarized glasses, which also affect the viewing experience.

In this paper, we focus on overcoming the above-mentioned limitations and improving the overall performance of the dual-view 3D display. To achieve this goal, we propose an II based dual-view 3D display which consists of a high-resolution display panel, a large-pitch lens array and a directional diffuser screen. The high-resolution display panel is used to display the elemental image array (EIA) including 3D information of two different 3D scenes. The large-pitch lens array is composed of a series of lenses with large diameter. The directional diffuser screen with specific diffusing angle is used to eliminate the gap between adjacent lenses and generate consecutive 3D images. Introducing the large-pitch lens array and high-resolution display panel enables us to improve both the viewing angle and 3D resolution of the dual-view 3D display. We also propose a projective transformation based pickup method to produce the EIA for the dual-view 3D display with high accuracy. We experimentally demonstrate a prototype of the proposed dual-view 3D display. The results show that our proposed system can display two different 3D images in different viewing zones with high quality.

2. Principle

2.1 Structure of the Proposed Dual-View 3D Display

Figure 1 shows the schematic of the proposed dual-view 3D display, which mainly consists of a display panel, a large-pitch lens array and a directional diffuser screen. The display panel shows the EIA synthesized from two sets of parallaxes, and each set represents different perspectives of one target 3D scene. The large-pitch lens array, including $M \times N$ plano-convex lenses, modulates the rays emitted by the pixels of the EIA and creates the perception of two different 3D scenes (e. g. point A of 3D scene 1, point B of 3D scene 2). The directional diffuser screen diffuses the rays emitted by the reconstructed 3D points with a specific diffusing angle to ensure that the observers can view consecutive 3D images [26], [27]. It locates at the given central depth plane (CDP) which is determined by the Gaussian imaging law. Then, different consecutive 3D images can be observed simultaneously in different viewing zones.
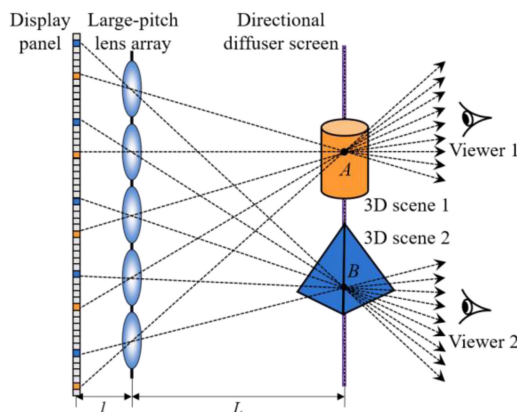
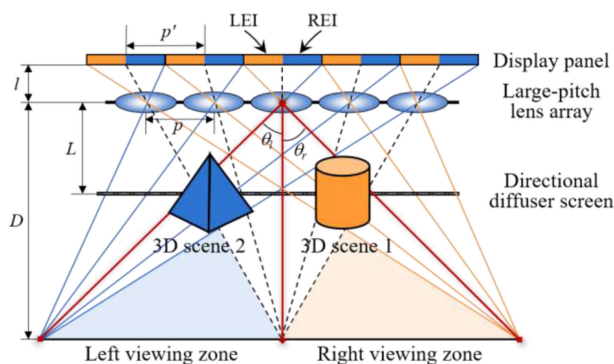Fig. 1. Schematic diagram of the proposed dual-view 3D display.

Fig. 2. Principle of the proposed dual-view 3D display in which the dimension of the EI is larger than the pitch of the lens array.

2.2 Principle of the Proposed Dual-View 3D Display

The most important concept of a dual-view 3D display is how to generate two different viewing zones. In the proposed system, we divide the EIA into two parts to produce a dual-view property. As shown in Fig. 2, each EI is divided into left elemental image (LEI) and right elemental image (REI). They are created from 3D scenes 1 and 2, respectively. Through the large-pitch lens array, each LEI or REI works as a spatially-incoherent object and they share the field of view of the corresponding lens. The conical ray bundles emitted by the pixels in the LEIs intersect and integrally reconstruct 3D scene 1 in the right viewing zone. Similarly, the conical ray bundles emitted by the pixels in the REIs intersect and reconstruct 3D scene 2 in the left viewing zone. Note that here we use the lenses to modulate the rays emitted by the pixels of the EIA instead of the micro-lenses. The diameter of the lenses used in the proposed dual-view 3D display is about 10 times larger than that of the micro-lenses used in the conventional dual-view II display. Compared with the conventional micro-lens, the lens can cover the LEI (or REI) with significantly improved pixels. Therefore, the viewing angle of each viewing zone can be significantly enlarged. In addition, adopting lenses can increase the number of the viewpoints and render a denser light field.

To further improve the viewing angles of the left and right viewing zones, we adopt a converge arrangement where the dimension of the EI is slightly larger than the pitch of the lens array [28]. For one-dimensional case, as illustrated in Fig. 2, p' stands for the dimension of the EI, and it can be calculated as:

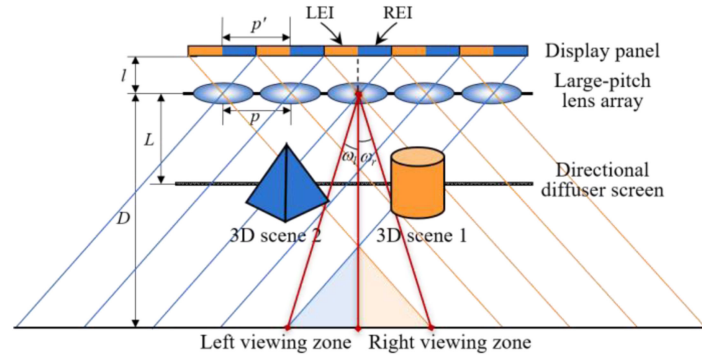$$p' = p \left(1 + \frac{l}{D} \right), \tag{1}$$

Fig. 3. Principle of the conventional dual-view 3D display in which the dimension of the EI and the pitch of the lens array are identical.

where p is the pitch of the lens array, D stands for the pre-set viewing distance, and l is the gap between the display panel and the lens array. At the pre-set viewing distance, the single viewing angles of all the lenses converge, and the flipping areas are also eliminated due to the convergence property. The viewing angle θ_l of the left viewing zone can be estimated by:

$$\theta_l = \arctan\left(\frac{p'}{2l}\right) = \arctan\left(\frac{p}{2l} + \frac{p}{2D}\right). \tag{2}$$

The viewing angle θ_r of the right viewing zone is the same as θ_l. As shown in Fig. 3, in the conventional arrangement where the dimension of the EI and the pitch of the lens array are identical, the viewing angles of the left and right viewing zones can be expressed as:

$$\omega_l = \omega_r = \arctan\left(\frac{p}{2l} - \frac{(U-1)p}{2D}\right), \tag{3}$$

where U is the number of the lenses. Obviously, θ_l (θ_r) is larger than the conventional viewing angle ω_l(ω_r). Note that the centers of the display panel and the large-pitch lens array are aligned in both horizontal and vertical directions to ensure the above-mentioned convergence.

Although the large-pitch lens array can successfully reproduce the light fields of 3D scenes 1 and 2 in different viewing zones, these light fields are discontinuous. The reason is that the gaps between adjacent lenses hinder the sampling for partial light rays, as shown in Fig. 4(a). Here we use a directional diffuser screen to remodulate the light distribution and produce the continuous light fields. The directional diffuser screen is a reception screen that can homogenize and directionally shape the emitted light within a specific diffusing angle. Note that the intensity of the diffusing light is inversely proportional to the diffusing angle and the incident angles. The diffusing angle is determined by the pseudo random and non-periodic structures carved on the surface of the directional diffuser screen. Since the lenses are symmetrically arranged, the diffusing angles should be consistent in horizontal and vertical directions.

For simplicity, we only analyze the reconstruction of 3D scene 2. The reconstruction of 3D scene 1 is similar to that of 3D scene 2. As shown in Fig. 4(b), when the directional diffuser screen is placed on the CDP, the pixel P_1 of the EI is regarded as a point source and emits a ray bundle R_1 which is refracted through the corresponding lens. Later, the ray bundle R_1 converges to the image point P' on the plane of the directional diffuser screen. The ray bundle R_2 emitted by the homonymy pixel P_2 of the adjacent EI also converges to the same point P'. Then, the point P' of the directional diffuser screen emits two ray bundles R_1' and R_2' in different directions with a controlled way, as if they are emitted from the point P' of the real 3D object. The continuous light field of 3D scene 2 can therefore be reproduced. Here the ray bundles R_1' and R_2' are the extension of the ray bundles R_1 and R_2 by the control of the diffusing angle φ. Therefore, the diffusing angle φ should be selected correctly. Considering the normal distribution characteristics of intensity of the
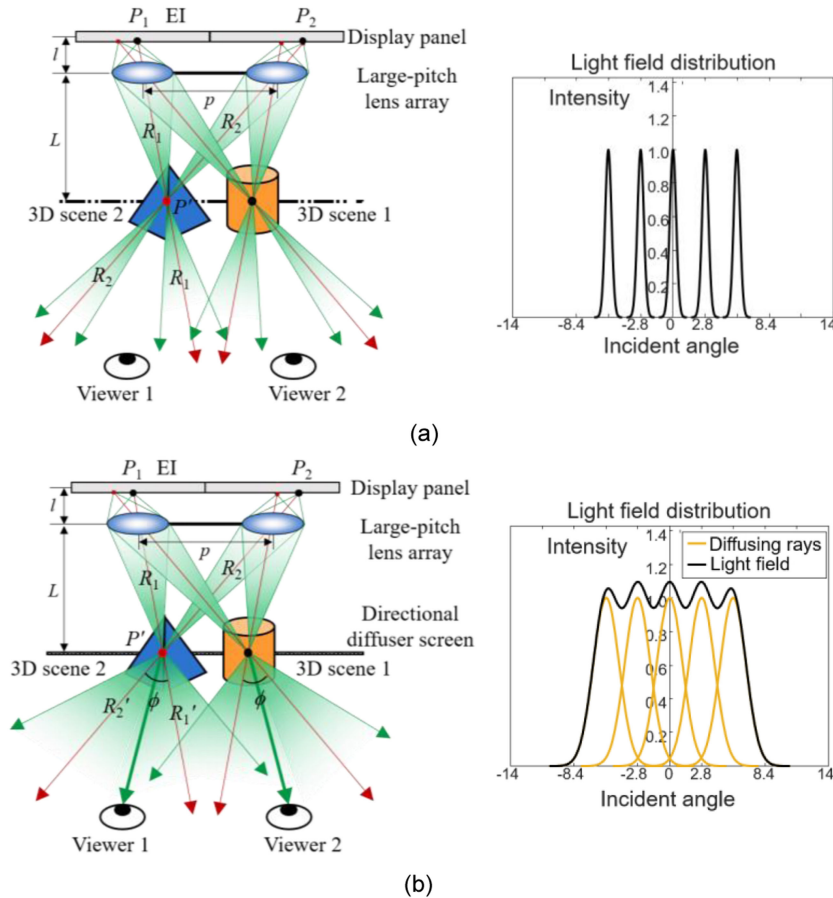
Fig. 4. Reconstructed light fields (a) without and (b) with the directional diffuser screen.

ray bundles, the diffusing angle φ is satisfied by:

$$\varphi = 2\arctan\left(\frac{p}{2L}\right). \tag{4}$$

The depth of field (DOF) of the proposed dual-view 3D display is the same as the conventional II display in real mode, which is evaluated in terms of the Rayleigh range. The DOF is defined as the distance between the front and rear marginal depth planes where the spot size equals the pixel size of the reconstructed image [29]. The front and rear marginal depth planes lie on both sides of the CDP. The DOF can be given by:

$$DOF = 2\frac{L^2 \Delta r}{ld}, \tag{5}$$

where d represents the diameter of the lens, Δr stands for the pixel size of the display panel. The diffraction effect of the lens array is disregarded. The DOF is proportional to the position of the CDP and the pixel size of the display panel, and inversely proportional to the diameter of the lens and the gap between the display panel and the large-pitch lens array. Thus, to realize a relatively large DOF, the tradeoff should be considered during the selection of the display parameters.

2.3 EIA Generation for the Proposed Dual-View 3D Display

As the inversion of the dual-view 3D display process, the pickup process should be analyzed with the similar principle as the display process. As shown in Fig. 5, during the display process, the
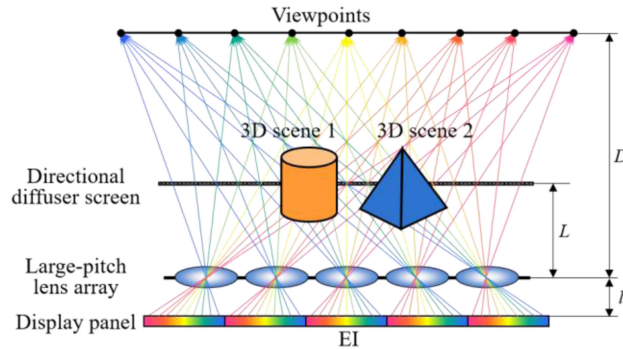
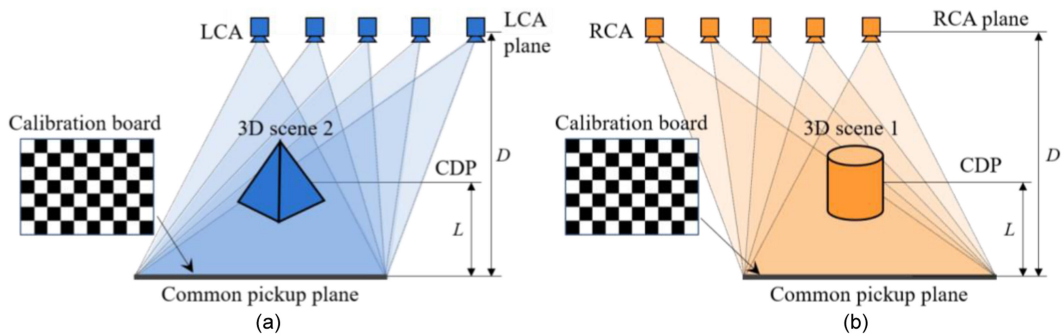Fig. 5. Rendered light fields during the display process.

Fig. 6. 3D scenes capturing from (a) LCA and (b) RCA.

rendered light fields can be decomposed into multiple sets of light field components. Half sets of the light field components are produced from 3D scene 1, and the other half correspond to 3D scene 2. Note that each set of the light field components can be obtained by an off-axis perspective projection from a specific viewpoint to one of the 3D scenes. The total number of the viewpoints is the same as the number of pixels per EI. Accordingly, in the pickup process, if we place two sets of off-axis cameras on the corresponding viewpoint positions, each camera can obtain an off-axis sub-image (SI) which is similar to one set of rendered light field components of the display process. Each off-axis SI contributes one pixel to a fixed position within each EI. However, the off-axis camera pickup is difficult to implement. In our proposal, we adopt the projective transformation to achieve an off-axis pickup effect.

The parameters of the pickup process are set to coincide with that of the display process. As shown in Fig. 6, we use two universal camera arrays, including left camera array (LCA) and right camera array (RCA), to capture 3D scenes 2 and 1, respectively. For simplicity, we explain the pickup principle in the LCA case. The pickup of the RCA is similar to that of the LCA. In the pickup, the total size of the LCA is equal to the effective size of the left viewing zone of the display process. In the horizontal direction, the number of the cameras of the LCA is equal to half the number of the pixels per EI, and it is denoted as M, where $M = p'/2\Delta r$. The number of the cameras of the LCA in the vertical direction is denoted as N, where $N = p'/\Delta r$. The optical axes of the cameras in the LCA could be parallel to each other. The LCA is placed at the distance D from the pickup plane.

In the ideal off-axis pickup, all cameras should have an exact same pickup plane. The width and height of this common pickup plane equal those of the large-pitch lens array of the display process, and they can be expressed as $(U\text{-}1)p$ and $(V\text{-}1)p$, respectively, where $U \times V$ is the number of the lenses of the display process. A calibration board is placed on the common pickup plane, and a chessboard pattern with $P \times Q$ interior corners is printed on the calibration board. By implementing a projective transformation from each cameras' pickup plane to the common pickup plane, the
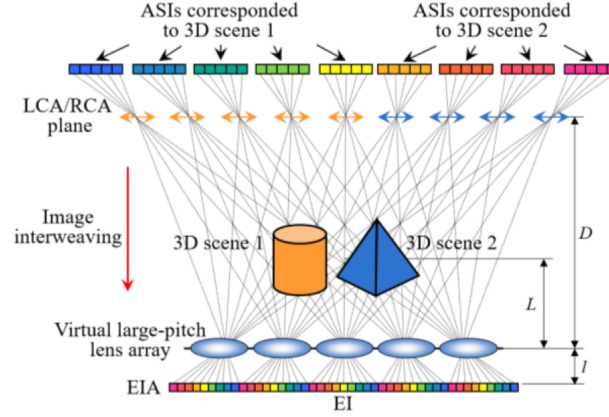
Fig. 7. EIA generation by interweaving two sets of ASIs.

off-axis pickup effect can be achieved. To ensure the accuracy of the projective transformation, the size of the interior region of the chessboard pattern should be equal to that of the common pickup plane. Thus, P and Q can be deduced as:

$$P = round\left(\frac{(U-1)p}{s}\right), \tag{6}$$

$$Q = round\left(\frac{(V-1)p}{s}\right), \tag{7}$$

where s represents the side length of the black/white squares of the chessboard pattern. The LCA only captures the calibration board firstly, and the recorded SIs are denoted as the chessboard images (CIs). Based on the coordinate detection about interior corners in each CI, the homography matrix $A_{m,n}$ of (m, n)-th camera can be calculated by the following constraint equation:

$$i_{m,n}\begin{bmatrix} x'_k \\ y'_k \\ 1 \end{bmatrix}_{m,n} = A_{m,n}\begin{bmatrix} x_t \\ y_t \\ 1 \end{bmatrix}_{m,n}, \tag{8}$$

where $A_{m,n}$ contains 3-by-3 elements, $i_{m,n}$ represents the scaling factor, $(x_t, y_t)_{m,n}$ is the corner locations of the CI captured by (m, n)-th camera, and $(x'_k, y'_k)_{m,n}$ is the vertex coordinates of the aligned sub-image (ASI) which is transformed by the SI captured by (m, n)-th camera. It requires 4 constraints of Eq. (8) to derive the homography matrix $A_{m,n}$: **1)** $t = 0$, $k = 0$, $(x'_0, y'_0)_{m,n} = (0, 0)$; **2)** $t = P \times (Q - 1)$, $k = 1$, $(x'_1, y'_1)_{m,n} = (0, R_V - 1)$; **3)** $t = P \times Q - 1$, $k = 2$, $(x'_2, y'_2)_{m,n} = (R_H - 1, R_V - 1)$; **4)** $t = P - 1$, $k = 3$, $(x'_3, y'_3)_{m,n} = (R_H - 1, 0)$, where $R_H \times R_V$ is the resolution of the EIA. After obtaining the homography matrices, the calibration board is removed and the LCA only captures 3D scene 2. The recorded SIs of 3D scene 2 are then be projected by using the corresponding homography matrices. Finally, the ASIs can be created with the same property as the off-axis SIs [30]. The ASIs have the same resolution as the EIA. ASIs of 3D scene 1 can also be generated by the similar procedure.

The EIA for the dual-view 3D display can be obtained by interweaving the ASIs corresponded to 3D scenes 1 and 2. As shown in Fig. 7, each ASI contributes one pixel to a fixed position within each EI. The ASI from (m, n)-th camera of the LCA is denoted as $L_{m,n}(x, y)$, and the ASI from

Fig. 8. Photograph of the proposed dual-view 3D display prototype.

(m, n)-th camera of the RCA is denoted as $R_{m,n}(x, y)$. The EIA $E(x, y)$ can be calculated as:

$$E(x, y) = \begin{cases} (\frac{p'}{\Delta r})^2 \sum\limits_{u,v} \sum\limits_{m,n} R_{m,n}(\frac{p'}{\Delta r}u + M - 1 - m, \frac{p'}{\Delta r}v + N - 1 - n)\delta \\ \left(x - \frac{p'}{\Delta r}u - M + 1 + m, y - \frac{p'}{\Delta r}v - N + 1 + n\right), \text{mod}(x, N) < M \\ (\frac{p'}{\Delta r})^2 \sum\limits_{u,v} \sum\limits_{m,n} L_{m,n}(\frac{p'}{\Delta r}u + N - 1 - m, \frac{p'}{\Delta r}v + N - 1 - n)\delta \\ \left(x - \frac{p'}{\Delta r}u - N + 1 + m, y - \frac{p'}{\Delta r}v - N + 1 + n\right), \text{mod}(x, N) \geq M \end{cases}, \quad (9)$$

where u and v are the indexes of the EI, $m = 0, 1, \ldots, M - 1$, $n = 0, 1, \ldots, N - 1$, and the symbol δ refers to Dirac delta function. Also, the pseudoscopic-orthoscopic image conversion is taken into consideration during the process of the EIA generation.

3. Experiments and Discussions

Figure 8 shows a photo of the proposed dual-view 3D display prototype. A 23.8-inch 60 Hz LCD (Dell P2415Q, with resolution 3840 × 2160) is used as the display panel. We embed 35 × 20 plano-convex lenses (GCL-010104, f12.7 mm, Ø12.7 mm, from Daheng Optics) in a perforated epoxy board to fabricate the large-pitch lens array. The pitch of the lens array is 14.7 mm. Considering that the intensity of the diffusing light is inversely proportional to the diffusing angle φ and the incident angles, the directional diffuser screen with smaller diffusing angle should be adopted. We use a directional diffuser screen (LSD, from Luminit Company) with circular diffusing angle of 5° × 5° in the proposed prototype. The directional diffuser screen is placed at a distance of 235 mm from the lens array. Following the Gaussian imaging law, the gap between the display panel and the large-pitch lens array is adjusted to 13.4 mm. The pre-set viewing distance is 2000 mm. The DOF of the proposed display system is 89.1 mm.

To demonstrate the performance of the dual-view 3D display, we start with building the LCA and RCA and capturing the calibration board individually. The LCA and RCA are located at the same depth plane, each of which consists of 54 × 108 virtual cameras. The calibration board is placed at a distance of 2000 mm from the LCA and RCA, as shown in Fig. 9(a). By detecting the coordinates of the chessboard corners in each CI and solving 4 constraint equations, the homography matrices can be calculated. Subsequently, we remove the calibration board and create two virtual 3D scenes consisting of the hand model for the left viewing zone and the wheel model for the right viewing zone. The depth of both models is set to 89 mm. The hand model is captured by the LCA with a distance of 1765 mm, and the wheel model is captured by the RCA with the same distance, as shown in Figs. 9(b) and 9(c), respectively. Note that the resolution of the obtained SIs should be consistent with that of the CIs. By performing the projective transformation to the captured SIs of the hand and wheel models, two sets of ASIs corresponded to the hand and wheel models can be generated. Figs. 10(a) and 11(a) show a portion of the SIs captured from the LCA and the corresponding ASIs, respectively. Figs. 10(b) and 11(b) show part of the SIs captured from the
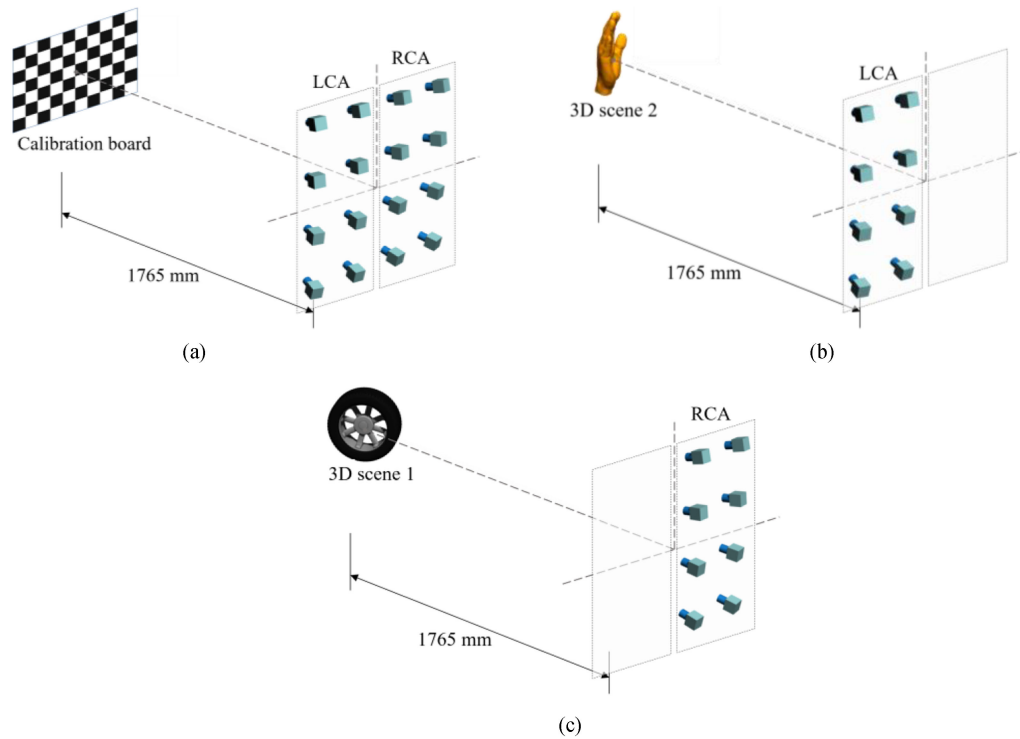
Fig. 9. Virtual 3D scenes and camera array. (a) Calibration board capturing from LCA and RCA, (b) 3D scene 2 capturing from LCA, and (c) 3D scene 1 capturing from RCA.
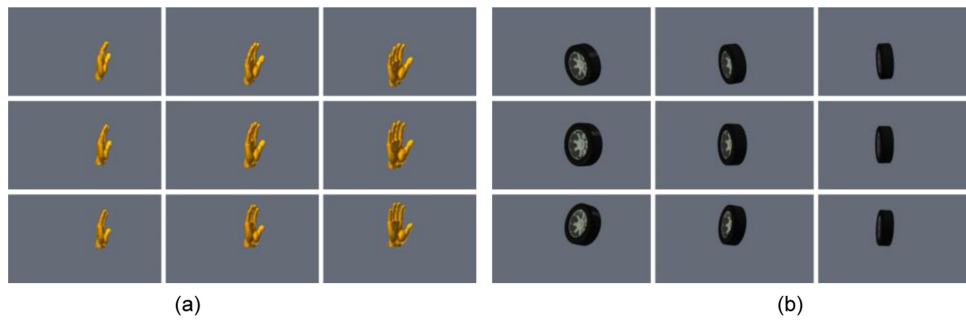

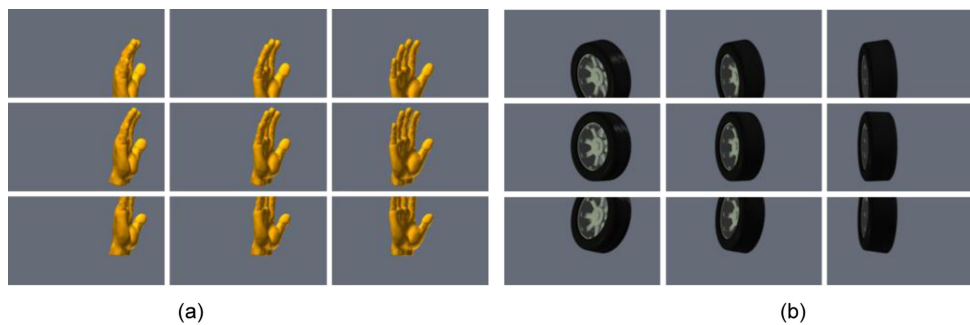Fig. 10. SIs obtained from (a) LCA and (b) RCA.

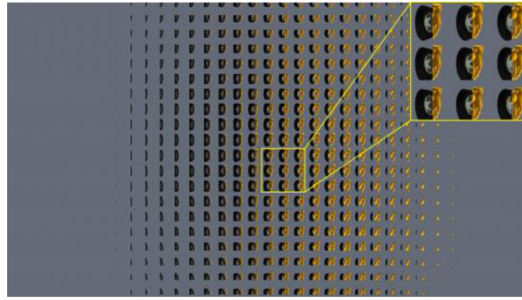Fig. 11. ASIs of (a) the hand model and (b) the wheel model.

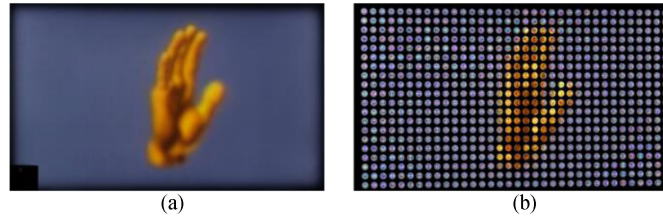Fig. 12. EIA for the proposed dual-view 3D display.

(a)   (b)

Fig. 13. Photos of the 3D image "hand" captured from the viewing angle of -17° (a) with and (b) without the directional diffuser screen.

(a) -26°   (b) -15°   (c) -3°

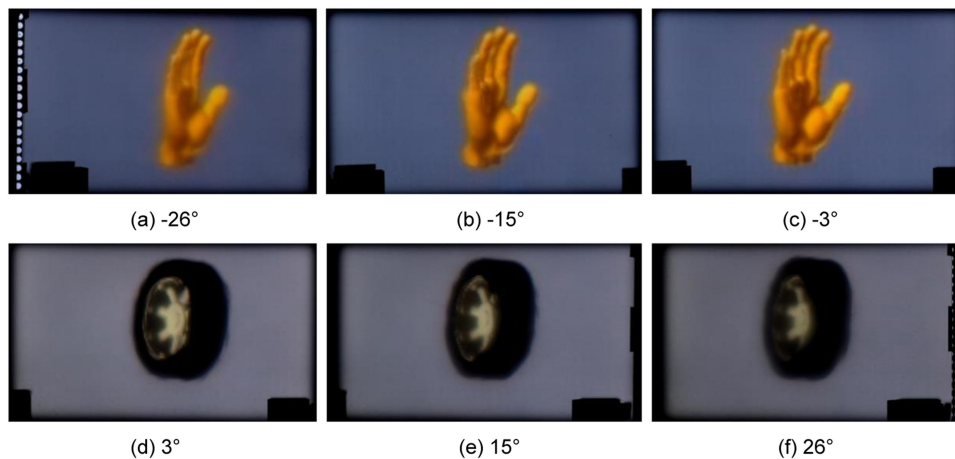(d) 3°   (e) 15°   (f) 26°

Fig. 14. Photos of the 3D images reconstructed by the proposed dual-view 3D display.

RCA and the corresponding ASIs, respectively. Since the interpolation occurs during the projective transformation process, the resolution of the SI and ASI looks different. Finally, we create the EIA with 3840×2160 pixels by interweaving the ASIs of the hand and wheel models, and the EIA is shown in Fig. 12.

To confirm the validity of the directional diffuser screen, we capture two photos of the 3D image "hand" with and without the directional diffuser screen, as shown in Figs. 13(a) and 13(b), respectively. Both photos are captured at the same viewing angle of -17°. It can be seen that the reconstructed 3D image is consecutive by introducing the directional diffuser screen.

Then, we perform the dual-view 3D display experiment. Fig. 14 shows the reconstructed 3D images at different viewing positions. The viewing angle for each 3D scene is 23°. As shown in Figs. 14(a) - 14(c), we can see different perspectives of 3D image "hand" from different viewing directions between -26° to -3° which is corresponded to the left viewing zone. While in the right viewing zone, as shown in Figs. 14(d) - 14(f), we can see different perspectives of 3D image "wheel"

from different viewing directions between 3° to 26°. Obviously, all sub-parts of the "hand/wheel" model have almost the same clarity. It can be deduced that the DOF of the display system is basically the same as the theoretical values of 89mm. However, the quality of the 3D images "wheel" and "hand" deteriorates with the increasing of the absolute value of the viewing angle. The reason is that the plano-convex lenses used in the proposed display manifest aberrations, and the aberrations become more serious with the enlargement of the viewing angle. Among the seven primary aberrations, the spherical aberration, the astigmatism and the coma aberration affect the quality of the 3D images mostly.

4. Conclusions

In this paper, we have presented an II based dual-view 3D display using a high-resolution display panel, a large-pitch lens array and a directional diffuser screen to enhance the viewing angle and the 3D image resolution. Based on the proposed architecture, two different 3D images can be reconstructed in different viewing zones simultaneously. We have demonstrated a prototype system that offers a viewing angle of 23° in each viewing zone and provides two different 3D images. The proposed display system has great potential application in automotive industry, medical field and so on. In our future work, we will focus on suppressing the aberrations of the reconstructed 3D images and further improving the viewing angle of each viewing zone.

References

[1] C. P. Chen, J. H. Lee, T. H. Yoon, and J. C. Kim, "Monoview/dual-view switchable liquid crystal display," *Opt. Lett.*, vol. 34, no. 14, pp. 2222–2224, 2009.

[2] C. T. Hsieh, J. N. Shu, H. T. Chen, C. Y. Huang, C. J. Tian, and C. H. Lin, "Dual-view liquid crystal display fabricated by patterned electrodes," *Opt. Exp.*, vol. 20, no. 8, pp. 8641–8648, 2012.

[3] J. P. Cui, Y. Li, J. Yan, H. C. Cheng, and Q. H. Wang, "Time-multiplexed dual-view display using a blue phase liquid crystal," *J. Display Technol.*, vol. 9, no. 2, pp. 87–90, 2013.

[4] C. P. Chen, Y. Wu, L. Zhou, K. Wang, Z. Zhang, and C. G. Jhun, "Crosstalk-free dual-view liquid crystal display using patterned E-type polarizer," *Appl. Opt.*, vol. 56, no. 3, pp. 380–384, 2017.

[5] D. U. Kean, D. J. Montgomery, G. Bourhill, and J. Mather, "Multiple view display," U.S. Patent 7154653B2, Dec. 6, 2006.

[6] M. P. C. M. Krijn, S. T. de Zwart, D. K. G. De Boer, O. H. Willemsen, and M. Sluijter, "2-D/3-D displays based on switchable lenticulars," *J. Soc. Inf. Display*, vol. 16, no. 8, pp. 847–855, 2008.

[7] J. Y. Son, V. V. Saveljev, Y. J. Choi, J. E. Bahn, H. H. Choi, and S. K. Kim, "Parameters for designing autostereoscopic imaging systems based on lenticular, parallax barrier and integral photography plates," *Opt. Eng.*, vol. 42, no. 11, pp. 3326–3333, 2003.

[8] J. Y. Luo, Q. H. Wang, W. X. Zhao, and D. H. Li, "Autostereoscopic three-dimensional display based on two parallax barriers," *Appl. Opt.*, vol. 50, no. 18, pp. 2911–2915, 2011.

[9] X. B. Yu *et al.*, "3D display with uniform resolution and low crosstalk based on two parallax interleaved barriers," *Chin. Opt. Lett.*, vol. 12, no. 12, 2014, Art. no. 121001.

[10] X. P. Li *et al.*, "Athermally photoreduced graphene oxides for three-dimensional holographic images," *Nature Commun.*, vol. 6, 2015, Art. no. 6984.

[11] A. Jones, I. McDowall, H. Yamada, M. Bolas, and P. Debevec, "Rendering for an interactive 360 light field display," *ACM Trans. Graph.*, vol. 26, no. 3, 2007, Art. no. 40.

[12] J. Y. Wu *et al.*, "Resolution enhanced light field near eye display using e-shifting method with birefringent plate," *J. Soc. Inf. Display*, vol. 26, no. 5, pp. 269–279, 2018.

[13] G. Tan, T. Zhan, Y. H. Lee, J. Xiong, and S. T. Wu, "Polarization-multiplexed multiplane display," *Opt. Lett.*, vol. 43, no. 22, pp. 5651–5654, 2018.

[14] T. Zhan, Y. H. Lee, and S. T. Wu, "High-resolution additive light field near-eye display by switchable Pancharatnam–Berry phase lenses," *Opt. Exp.*, vol. 26, no. 4, pp. 4863–4872, 2018.

[15] G. Lippmann, "La photographie integrale," *Comptes Rendus Academie Sci.*, vol. 146, pp. 446–451, 1908.

[16] H. Arimoto and B. Javidi, "Integral three-dimensional imaging with digital reconstruction," *Opt. Lett.*, vol. 26, no. 3, pp. 157–159, 2001.

[17] X. Xiao, B. Javidi, M. Martínez-Corral, and A. Stern, "Advances in three-dimensional integral imaging: Sensing, display, and applications," *Appl. Opt.*, vol. 52, no. 4, pp. 546–560, 2013.

[18] B. Javidi, J. Sola-Pikabea, and M. Martinez-Corral, "Recent advances in 3-D integral imaging sensing and display," *IEEE Photon. J.*, vol. 7, no. 3, pp. 1–7, Jun. 2015.

[19] X. W. Li, L. Li, and Q. H. Wang, "Wavelet-based iterative perfect reconstruction in computational integral imaging," *J. Opt. Soc. Amer. A*, vol. 35, no. 7, pp. 1212–1220, 2018.

[20] G. D. Love, D. M. Hoffman, P. J. W. Hands, J. Gao, A. K. Kirby, and M. S. Banks, "High-speed switchable lens enables the development of a volumetric stereoscopic display," *Opt. Exp.*, vol. 17, no. 18, pp. 15716–15725, 2009.

[21] F. Wu, H. Deng, C. G. Luo, D. H. Li, and Q. H. Wang, "Dual-view integral imaging three-dimensional display," *Appl. Opt.*, vol. 52, no. 20, pp. 4911–4914, 2013.

[22] F. Wu, Q. H. Wang, C. G. Luo, D. H. Li, and H. Deng, "Dual-view integral imaging 3D display using polarizer parallax barriers," *Appl. Opt.*, vol. 53, no. 10, pp. 2037–2039, 2014.

[23] J. Jeong, C. K. Lee, K. Hong, J. Yeom, and B. Lee, "Projection-type dual-view three-dimensional display system based on integral imaging," *Appl. Opt.*, vol. 53, no. 27, pp. G12–G18, 2014.

[24] Q. H. Wang, C. C. Ji, L. Li, and H. Deng, "Dual-view integral imaging 3D display by using orthogonal polarizer array and polarization switcher," *Opt. Exp.*, vol. 24, no. 1, pp. 9–16, 2016.

[25] F. Wu, G. J. Lv, H. Deng, B. C. Zhao, and Q. H. Wang, "Dual-view integral imaging three-dimensional display using polarized glasses," *Appl. Opt.*, vol. 57, no. 6, pp. 1447–1449, 2018.

[26] J. H. Lee, J. Park, D. Nam, S. Y. Choi, D. S. Park, and C. Y. Kim, "Optimal projector configuration design for 300-Mpixel multi-projection 3D display," *Opt. Exp.*, vol. 21, no. 22, pp. 26820–26835, 2013.

[27] X. Z. Sang, X. Gao, X. B. Yu, S. J. Xing, Y. H. Li, and Y. L. Wu, "Interactive floating full-parallax digital three-dimensional light-field display based on wavefront recomposing," *Opt. Exp.*, vol. 26, no. 7, pp. 8883–8889, 2018.

[28] H. Deng, Q. H. Wang, L. Li, and D. H. Li, "An integral-imaging three-dimensional display with wide viewing angle," *J. Soc. Inf. Display*, vol. 19, no. 10, pp. 679–684, 2011.

[29] S. W. Min, J. Kim, and B. Lee, "New characteristic equation of three-dimensional integral imaging system and its applications," *Japanese J. Appl. Phys.*, vol. 44, no. 2, pp. L71–L74, 2005.

[30] Z. L. Xiong, Y. Xing, H. Deng, and Q. H. Wang, "Planar parallax based camera array calibration method for integral imaging three-dimensional information acquirement," *SID Int. Symp. Dig. Tech. Paper*, vol. 47, no. 1, pp. 219–222, 2016.